

PNNL-38463

## Autonomous Flow Electrochemistry for Accelerated Catalyst Discovery

## September 2025

Soumya Vasisht
Eric Wiedner
Juan Lopez-Ruiz
Nathanael Royer
Talshyn Begildayeva
Sutanay Choudhury
James Koch
Rahul Birmiwal
Zimo Wang
Nancy Washton



#### DISCLAIMER

This report was prepared as an account of work sponsored by an agency of the United States Government. Neither the United States Government nor any agency thereof, nor Battelle Memorial Institute, nor any of their employees, makes any warranty, express or implied, or assumes any legal liability or responsibility for the accuracy, completeness, or usefulness of any information, apparatus, product, or process disclosed, or represents that its use would not infringe privately owned rights. Reference herein to any specific commercial product, process, or service by trade name, trademark, manufacturer, or otherwise does not necessarily constitute or imply its endorsement, recommendation, or favoring by the United States Government or any agency thereof, or Battelle Memorial Institute. The views and opinions of authors expressed herein do not necessarily state or reflect those of the United States Government or any agency thereof.

PACIFIC NORTHWEST NATIONAL LABORATORY

operated by

BATTELLE

for the

UNITED STATES DEPARTMENT OF ENERGY

under Contract DE-AC05-76RL01830

Printed in the United States of America

Available to DOE and DOE contractors from the Office of Scientific and Technical Information, P.O. Box 62, Oak Ridge, TN 37831-0062

ph: (865) 576-8401 fox: (865) 576-5728 email: reports@osti.gov

Available to the public from the National Technical Information Service 5301 Shawnee Rd., Alexandria, VA 22312 ph: (800) 553-NTIS (6847) or (703) 605-6000

email: <a href="mailto:info@ntis.gov">info@ntis.gov</a>
Online ordering: <a href="http://www.ntis.gov">http://www.ntis.gov</a>

# **Autonomous Flow Electrochemistry for Accelerated Catalyst Discovery**

September 2025

Soumya Vasisht
Eric Wiedner
Juan Lopez-Ruiz
Nathanael Royer
Talshyn Begildayeva
Sutanay Choudhury
James Koch
Rahul Birmiwal
Zimo Wang
Nancy Washton

Prepared for the U.S. Department of Energy under Contract DE-AC05-76RL01830

Pacific Northwest National Laboratory Richland, Washington 99354

### **Abstract**

Our objective is to develop an Autonomous Chemical Experimentation (ACE) platform that accelerates discovery of new catalytic transformations and other energy-relevant chemical reactions and processes. We intentionally designed ACE to be highly modular, both with respect to its rapid deployment to different chemistries and experimental workflows as well as incorporation of a wide range of different AI algorithms. In addition to the development of the core software architecture, initial efforts were made to incorporate Large Language Models to provide human-interpretable reasoning of the optimizer's actions, and to develop a user-friendly graphical interface for experimental researchers. ACE was demonstrated using a flow electrocatalysis platform containing an inline FTIR spectrometer for real-time analysis and quantification of the reaction outcome. Human-in-the-loop experiments were performed in which a human researcher conducted an experiment using electrode potentials suggested by ACE, then fed the spectral data back to ACE for decision making. After confirming the successful function of the optimizer, efforts were next directed to automation of the hardware and performed full autonomy tests using three reactions: catalytic oxidation of formate, catalytic oxidation of cyclohexanol, and oxidation of hydroguinone. These studies confirm that ACE can close the loop between reaction execution. analysis, and optimization. They also reveal that more improved product detection methods will be essential for ACE to make well-informed decisions for reactions with low conversions.

Abstract

## **Acknowledgments**

This research was supported by the Physical and Computational Science Directorate Mission Seed, under the Laboratory Directed Research and Development (LDRD) Program at Pacific Northwest National Laboratory (PNNL). PNNL is a multi-program national laboratory operated for the U.S. Department of Energy (DOE) by Battelle Memorial Institute under Contract No. DE-AC05-76RL01830.

Acknowledgments

## **Acronyms and Abbreviations**

ACE Autonomous Chemical Experimentation

API Application Programming Interface

ATR Attenuated Total Reflectance

CE Counter Electrode

EI Expected Improvement
FTIR Fourier Transform Infrared

FY Fiscal Year

GP Gaussian Process

I/O Input-Output IR Infrared

LLM Large Language Model
PI Probability of Improvement

RE Reference Electrode
RTU Remote Terminal Unit
UCB Upper Confidence Bound

UX User Experience
WE Working Electrode

## **Contents**

Abstra	act			i		
Ackno	wledgr	nents		ii		
Acron	yms ar	d Abbrev	viations	i\		
1.0	Introduction					
	1.1	1.1 Levels of Autonomy				
2.0	Reactor Design and Automation					
	2.1	2.1 Batch Reactor for L3 Autonomy (FY24)				
	2.2	Flow Reactor for L4 Autonomy (FY25)				
	2.3	Flow Reactor Automation				
		2.3.1	Electrochemical Control: Biologic VSP3e Potentiostat	5		
		2.3.2	Temperature Control: Autonics Multi-Channel Controller	5		
		2.3.3	Spectroscopic Analysis: Mettler Toledo ReactlR FTIR Spectrometer	6		
3.0	Softw	are Arch	itecture and Algorithms	7		
	3.1	ACE C	omputational Architecture	7		
	3.2	Optimiz	Optimization Algorithm Integration			
		3.2.1	Bayesian optimization	9		
4.0	Large Language Models (LLMs) for Experiment Interpretation					
	4.1	Spectral Data Interpretation1				
	4.2	Suggesting Experimental Steps12				
5.0	User	Experien	ce (UX) Design	14		
6.0	Model Chemistries					
	6.1	Formate Oxidation15				
	6.2	Cycloh	exanol Oxidation	16		
	6.3	Hydroquinone Oxidation1				
7.0	Expe	rimentatio	on Procedure	18		
	7.1	Human-in-the-loop Experimentation (FY 24)18				
	7.2	Autonomous Experimentation19				
8.0	Key C	Optimizat	ion Metrics	21		
	8.1	Produc	ct Yield	21		
	8.2	Farada	aic Efficiency	21		
	8.3	Selecti	vity	22		
	8.4	8.4 Reaction Rate				
9.0	Key Results					
	9.1	FY24 (Level 3) Human-in-the-loop experimentation2				
	9.2	FY25 (	Level 4) Autonomous Experimentation	24		
10.0	Conc	lusion		26		

11.0	References	2	>
11.0		4	_ /

Contents

## **Figures**

Figure 1: (a) Typical batch reactor setup, (b) Schematic of the batch reactor used for the formate chemistry. This batch reactor was used to demonstrate L3  Autonomy (Human-in-the-loop experimentation)	3
Figure 2: Schematic diagram of the flow reactor setup.	4
Figure 3: Photograph of the assembled electrochemical reactor platform showing: (a) liquid pumps, (b) liquid pre-heating loop, (c) electrochemical flow cell, (d) electronic control panel for liquid pumps, (e) ReactIR equipped with a flow detector, (f) potentiostat (not shown)	4
Figure 4: Biologic VSP3e multichannel potentiostat	5
Figure 5: Autonics TM series temperature controller	5
Figure 6: Mettler Toledo ReactIR in-situ FTIR spectrometer	6
Figure 7: ACE is a modular architecture that will serve as an interface between real- world physical experimentation and modern numerical methods in data science and optimization	7
Figure 8. Bayesian optimization uses a surrogate model and an acquisition function to guide the search for optimal experiment conditions. Figure from ax.dev	9
Figure 9. Expert evaluation of Al-extracted spectral features for cyclohexanol system	12
Figure 10. Screenshots of design concepts for the experiment specification page and the real-time dashboard.	14
Figure 11. Depiction of the anode reactions selected for testing the autonomous electrochemistry platform. In each case, the corresponding cathode reaction is hydrogen evolution	15
Figure 12: Calibration curves obtained from FTIR response for known concentrations of potassium formate (left) and potassium bi-carbonate (right) aqueous solutions.	16
Figure 13: Calibration curves obtained from FTIR response for known concentrations of cyclohexanone aqueous solutions	17
Figure 14: Calibration curves obtained from FTIR response for known concentrations of hydroquinone (left) and benzoquinone (right) aqueous solutions	17
Figure 15: Human-in-the-loop, semi-autonomous workflow with two distinct points of human intervention	18
Figure 16: Fully autonomous workflow with direct instrument control	19
Figure 17: Product quantification and key metrics of catalytic formate oxidation, showing the time dependence of FTIR signal intensity (top left), calculated concentrations (top right), and the catalytic metrics of Product Yield and Faradaic Efficiency (bottom)	23
Figure 18: Evolution of Gaussian process surrogate model used by the multi-objective Bayesian optimization algorithm. After 8 runs, the optimal potential was found around 0.36V	24

Figures

Figures

### 1.0 Introduction

Catalysts will play a key role in strengthening America's energy and manufacturing resilience. Catalytic processes, integral to modern society, contribute approximately 25% to the U.S. GDP and underpin essential consumer goods production. Fundamental catalysis research is essential to develop new chemical technologies that use abundant yet distributed domestic resources of energy-rich carbon feedstocks to produce chemicals and fuels. One powerful approach is electrocatalysis, in which electric current is used to promote bond breaking and bond forming, thereby enabling new reaction pathways and enhanced selectivity. However, discovery of new catalysts – spanning both synthesis and testing of potential materials – is very labor-intensive and demands meticulous adjustment of variables, with physical conditions and chemical environments significantly influencing outcomes. Electrocatalysis adds further complications through the need to develop catalysts for both anodic and cathodic reactions, each with their unique synthesis and evaluation requirements.

The development of autonomous experimental systems represents a transformative solution to these challenges, enabling the systematic exploration of complex parameter spaces with unprecedented efficiency and objectivity. Traditional electrochemical optimization approaches rely heavily on human intuition, sequential one-factor-at-a-time methodologies, and labor-intensive experimental studies that often fail to capture the intricate relationships between multiple variables. The exponential growth in computational capabilities, coupled with advances in machine learning algorithms and laboratory automation, has created unique opportunities to fundamentally reimagine how chemical discovery and process optimization are conducted.

The Autonomous Chemical Experimentation (ACE) platform was developed to address these limitations by creating a fully integrated system capable of autonomous experimental design, execution, and optimization for electrochemical processes. ACE combines sophisticated instrument control, real-time analytical monitoring, and artificial intelligence-driven decision-making to enable unattended optimization studies that can operate continuously for days or weeks. The platform specifically targets flow electrocatalysis applications, where the complex interplay between voltage, temperature, flow rates, and chemical composition requires systematic exploration of multidimensional parameter spaces to identify optimal operating conditions.

This report presents the comprehensive development and validation of ACE through multiple electrochemical investigations, focusing on the transition from human-in-the-loop semi-autonomous operation to fully autonomous experimentation. Key innovations include a modular software architecture that enables rapid adaptation to new chemistry domains, integration of large language models for experimental interpretation and decision explanation, and the implementation of Bayesian optimization algorithms specifically tailored for expensive electrochemical function evaluations. The platform incorporates real-time FTIR spectroscopy for product quantification, automated electrochemical characterization, and multi-objective optimization considering product yield, Faradaic efficiency, selectivity, and reaction rates.

The technical contributions span hardware integration challenges, signal processing methodologies for low-concentration product detection, autonomous experimental protocols, and user experience design for complex scientific workflows. Through systematic testing across three distinct electrochemical systems — potassium formate oxidation, alcohol oxidation, and hydroquinone oxidation — ACE successfully narrowed the search space while maintaining rigorous experimental standards and data quality. However, the platform's ultimate identification of optimal operating conditions was limited by the detection limit of the FTIR spectrometer. These findings underscore both the promise of the autonomous approach and the technical challenges

Introduction 1

that must be overcome for investigation of emerging catalysis applications without known solutions. The project's impact extends beyond technical achievements, having resulted in community recognition through workshops at Los Alamos National Laboratory and Argonne National Laboratory, securing follow-on funding from the Department of Energy Advanced Scientific Computing Research program, and generating significant interest from internal research groups seeking collaborative opportunities for autonomous experimentation applications.

### 1.1 Levels of Autonomy

The development of autonomous experimental systems requires a clear framework for defining and measuring the degree of independence from human intervention. Building upon established autonomy classifications, a six-level framework, given in the Autonomous Science initiative funding call, was used as a guidance for our ideation and development. It distinguishes between automation (physically-situated tools performing repetitive, pre-planned actions) and autonomous systems (able to accomplish tasks with minimal human involvement while predicting, planning, and adapting to environmental changes).

- **Level 0 No Autonomy:** Traditional manual experimentation where humans perform all tasks without automation support, representing the current state of most research laboratories.
- **Level 1 Assistance:** Human-executed experimental plans assisted by automated devices for repetitive, simple, and well-defined tasks such as pipetting robots or data logging instruments.
- **Level 2 Task Autonomy:** Human-executed plans supported at each step by automated data analysis and decision tools based on predefined criteria, enabling enhanced efficiency while maintaining human oversight of all major decisions.
- **Level 3 Conditional Autonomy:** Human-defined experimental plans with closed-loop semiautomated execution, where systems incrementally optimize plans based on results while requiring human intervention for anomalies or significant deviations.
- **Level 4 High Autonomy:** Fully automated execution of human-designed experimental plans, including integrated safety constraints and continuous operation without human intervention once initiated.
- **Level 5 Full Autonomy:** Human-defined goals with instrument or laboratory systems that independently develop, execute, and adapt experimental plans to achieve objectives, potentially suggesting new research directions.

The ACE platform was specifically designed to demonstrate both Level 3 (conditional autonomy) and Level 4 (high autonomy) capabilities for electrochemical optimization. The human-in-the-loop configuration exemplifies Level 3 autonomy, where researchers define experimental objectives and parameter spaces while ACE executes closed-loop optimization with minimal human intervention for instrument configuration and data management. The fully autonomous configuration achieves Level 4 autonomy through complete elimination of human intervention during plan execution, enabling unattended optimization cycles over long durations.

Introduction 2

## 2.0 Reactor Design and Automation

## 2.1 Batch Reactor for L3 Autonomy (FY24)

In FY24 we employed an electrochemical batch reactor to test the implementation of L3 autonomy prior to moving forward with efforts to achieve L4 autonomy. This batch reactor was a standard three-electrode (working electrode [WE], reference electrode [RE], and counter electrode [CE]) set up in undivided cell with a fixed volume of electrolyte solution and was operated manually to record the outcomes of the experiments suggested by ACE (L3 autonomy) (Figure 1).

Figure 1: (a) Typical batch reactor setup, (b) Schematic of the batch reactor used for the formate chemistry. This batch reactor was used to demonstrate L3 Autonomy (Human-in-the-loop experimentation).

## 2.2 Flow Reactor for L4 Autonomy (FY25)

In FY25 we employed a flow electrocatalysis platform that was previously developed by members of our team (Figures 2-3).<sup>1-4</sup> This flow cell consists of two compartments – namely, an anode and a cathode – separated by a Nafion 117 proton exchange membrane (PEM). A reference electrode (RHE) is positioned in the anodic compartment. A titanium (Ti) plate serves as the anode (i.e., WE), while a platinized titanium (Pt/Ti) plate functions as the cathode (i.e., CE). The electrolyzer is equipped with heating pads attached to the cathode and anode plates, as well as a pre-heating loop designed to warm the electrolyte before it enters the cell. The system operates using a flow-by configuration and functions in single-pass mode. Electrolyte is delivered to the cell compartments by two peristaltic pumps at a flow rate of 4 to 5 mL/min. The outlet of the anode compartment, where the reaction of interest occurs, is connected to a reactIR spectrometer unit for monitoring reaction progress; the solution leaving the spectrometer unit is routed to a waste container. Similarly, the outlet of the cathode compartment is also directed to the same waste

container. This flow reactor setup was selected since it possesses the basic functions needed for L4 autonomy: controllable stimulus to impact the reaction performance (temperature and potential), and a low-latency detector for monitoring the reaction outcome in real-time (reactIR spectrometer).

Figure 2: Schematic diagram of the flow reactor setup.



Figure 3: Photograph of the assembled electrochemical reactor platform showing: (a) liquid pumps, (b) liquid pre-heating loop, (c) electrochemical flow cell, (d) electronic control panel for liquid pumps, (e) ReactIR equipped with a flow detector, (f) potentiostat (not shown).

### 2.3 Flow Reactor Automation

The ACE platform integrated multiple specialized instruments to enable fully autonomous electrochemical experimentation. Each instrument was implemented as either an actuator (capable of changing experimental conditions) or sensor (monitoring system state) with dedicated communication strategies tailored to the manufacturer's available interfaces and protocols.

### 2.3.1 Electrochemical Control: Biologic VSP3e Potentiostat

The Biologic VSP3e multichannel potentiostat served as the primary electrochemical control instrument, functioning as both an actuator and sensor. As an actuator, it controlled applied voltage and electrochemical techniques (cyclic voltammetry, chronoamperometry). As a sensor, it continuously monitored electrochemical responses including current, voltage, and impedance measurements.

**Communication Strategy:** Biologic provides a comprehensive developer package with native Python API support, enabling direct programmatic control. Additionally, the third-party open-source package "easy-biologic" offered simplified Python wrappers that streamlined common electrochemical operations. The Python integration enabled



Figure 4: Biologic VSP3e multichannel potentiostat

real-time parameter adjustment based on experimental feedback, supporting the autonomous decision-making loop.

### 2.3.2 Temperature Control: Autonics Multi-Channel Controller

The Autonics multichannel temperature controller functioned primarily as an actuator for maintaining precise thermal conditions throughout the flow reactor system. The instrument featured built-in PID (Proportional-Integral-Derivative) controller that automatically adjusted heating output to maintain target setpoints, reducing temperature fluctuations that could affect reaction kinetics and product selectivity.

**Communication Strategy:** Communication was established using the Modbus RTU protocol, an industrial standard for serial communication between electronic devices. Modbus RTU transmits binary data in a compact format, making it suitable for real-time control applications. ACE implemented this



Figure 5: Autonics TM series temperature controller

communication using the "minimalmodbus" Python package, which provided straightforward read/write operations to the controller's input registers. This approach allowed ACE to remotely update temperature setpoints and monitor actual temperatures, ensuring thermal equilibrium before data collection phases.

### 2.3.3 Spectroscopic Analysis: Mettler Toledo ReactIR FTIR Spectrometer

The ReactIR in-situ FTIR spectrometer functioned exclusively as a sensor, providing real-time chemical composition analysis of the flowing reaction mixture. The instrument used attenuated total reflectance (ATR) sampling to monitor molecular vibrations, enabling identification and quantification of reactants, products, and intermediates without sample removal or preparation.

**Communication Strategy:** Unlike the other instruments, the ReactIR lacked direct Python API support, necessitating an indirect automation approach. The instrument's proprietary software was configured to



Figure 6: Mettler Toledo ReactIR in-situ FTIR spectrometer

automatically save spectral data at predetermined intervals (typically every 10 seconds during data collection phases) to a designated network-accessible directory. ACE implemented a custom Filel/O communication strategy that continuously monitored this directory for new spectral files. Upon detection of new data files, ACE's data processing modules automatically imported, preprocessed, and analyzed the spectral information. This file-based communication strategy proved robust and eliminated potential instrument control conflicts between ACE and the manufacturer's software.

The integration of these three instrument communication strategies—direct API control, industrial protocol communication, and file-based data exchange—demonstrates the flexibility required for heterogeneous laboratory automation where instruments from different manufacturers may use incompatible communication standards.

## 3.0 Software Architecture and Algorithms

## 3.1 ACE Computational Architecture

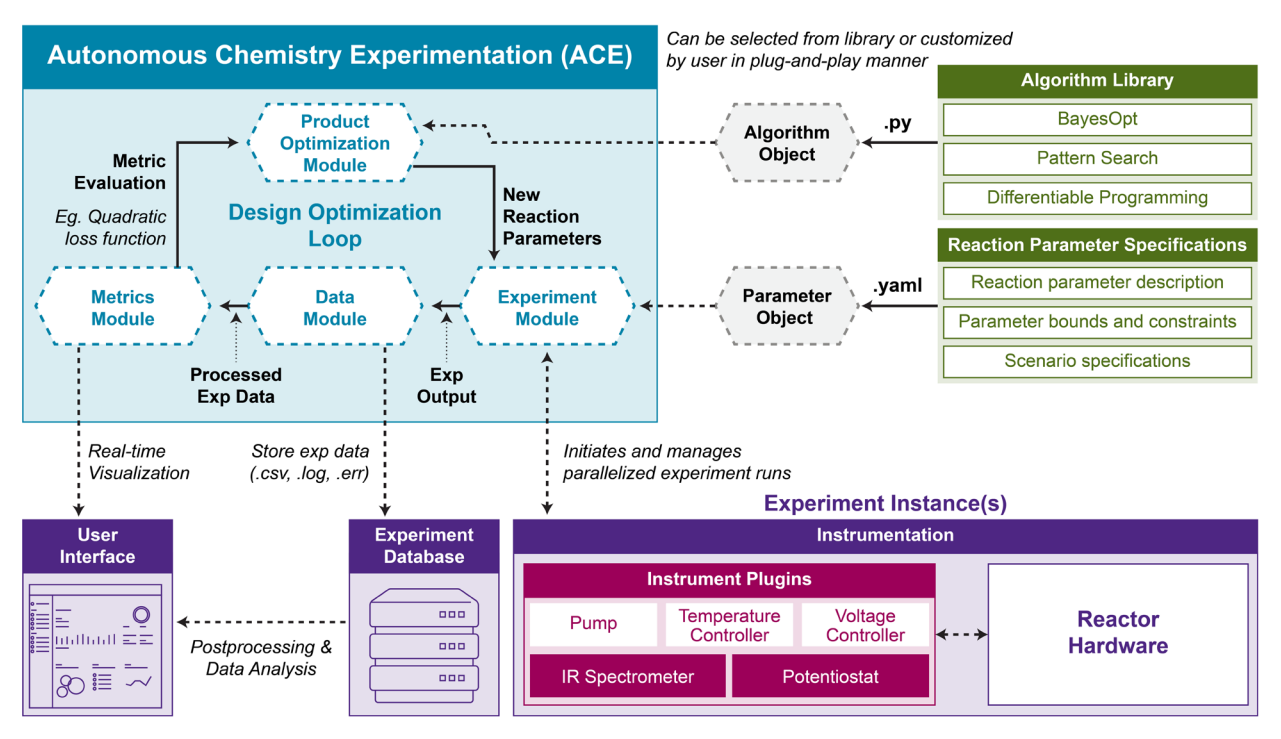


Figure 7: ACE is a modular architecture that will serve as an interface between real-world physical experimentation and modern numerical methods in data science and optimization.

ACE employs a modular architecture built around a core set of base modules that implement standardized, consistent APIs to ensure compatibility across diverse experimental workflows and optimization algorithms. ACE supports semi-autonomous and fully autonomous experimentation. This design philosophy enables seamless integration with various laboratory instruments while maintaining flexibility for different research domains and experimental objectives. By using a module-based architecture (Figure 7), ACE is designed to be easily reconfigured for a wide range of experimental workflows beyond the initial demonstration in flow electrolysis in this project.

The architecture consists of two primary layers: **base modules** that provide standardized functionality, and **flexible modules** that enable customization for specific use cases. Configuration is managed through YAML files that define experimental design parameters, including variable bounds, constraints, and target metrics such as product yield, current efficiency, selectivity, and reaction rates. Custom Python scripts handle metric computation and experimental data processing, allowing researchers to implement domain-specific calculations while maintaining compatibility with the broader ACE framework. This approach allows users to define new experimental campaigns without modifying the core architecture.

The base modules consist of:

 Experiment Module: Provides unified support for both simulated and empirical experiments through standardized APIs. The module defines consistent interfaces for specifying actuator inputs (experimental parameters) and collecting sensor outputs (measured responses), enabling seamless switching between computational models and physical experiments.

- **Data Module:** Implements standard data types and processing methodologies, including templates for custom data manipulation. This module ensures consistent data formatting and provides preprocessing capabilities that prepare raw instrument outputs for downstream analysis.
- Metrics Module: Receives processed experimental data and evaluates key performance indicators and objectives for given input conditions. The module produces structured, Al-ready outputs that enable optimization algorithms to train and update their internal models efficiently.
- **Optimizer Module:** Integrates new data from the metrics module to update predictive models and identify optimal parameters for subsequent experiments. The module communicates directly with the experiment module to execute instrument control commands, completing the autonomous experimentation loop.

The flexible modules consist of:

- YAML Configuration File: New experiments are specified using intuitive key-value pairs that define the complete experimental setup. The parameter space section specifies all controllable variables along with their feasible ranges, constraints, and data types. Fixed variables and metadata that remain constant throughout the optimization cycle are declared separately, ensuring consistent experimental conditions while allowing the optimizer to explore the defined parameter space. The configuration file also specifies target metrics and objectives, including whether each metric should be minimized or maximized. ACE supports both multi-objective optimization scenarios, where multiple competing objectives are simultaneously considered, and single-objective approaches where multiple metrics are combined into a weighted sum. This flexibility accommodates diverse research goals, for example, maximizing product yield while minimizing energy consumption to achieving optimal trade-offs between reaction rate and selectivity.
- Custom Processing Integration: Each experiment configuration is paired with a Python script that implements domain-specific data processing modules and metrics computation subroutines. These scripts define how raw instrument data should be transformed, filtered, and analyzed to extract meaningful performance indicators. The modular design ensures that custom processing logic integrates seamlessly with the standardized data flow, enabling researchers to implement specialized calculations for novel chemistry or unconventional measurement techniques while maintaining compatibility with ACE's optimization algorithms.

## 3.2 Optimization Algorithm Integration

ACE incorporates multiple data-driven optimization methods through standardized interfaces, including Bayesian optimization, pattern search, and differentiable programming approaches. Users can select algorithms based on their specific requirements during implementation. Future development will focus on creating automated algorithm selection mechanisms that choose the most appropriate optimization method based on problem characteristics. Current testing has concentrated on Bayesian optimization across the implemented chemistries; therefore, the following section elaborates specifically on this optimization framework.

### 3.2.1 Bayesian optimization

Bayesian optimization is a sequential model-based approach for optimizing expensive-to-evaluate functions, making it particularly well-suited for autonomous experimentation where each measurement is generally expensive to obtain, requiring significant time and resources. The method constructs a probabilistic surrogate model, typically a Gaussian process (GP) or a random forest, that captures both the predicted response and associated uncertainty across the parameter space. This probabilistic framework enables the algorithm to make informed decisions about where to sample next by balancing exploration of uncertain regions with exploitation of promising areas.

For chemical experimentation, Bayesian optimization offers several advantages over traditional optimization methods. It naturally handles noisy measurements common in experimental systems, requires relatively few function evaluations to find optimal conditions, and provides uncertainty quantification that helps identify regions where additional experiments would be most informative. The method is particularly effective for problems with expensive function evaluations, continuous parameter spaces, and limited prior knowledge about the underlying response surface, making it an ideal choice for autonomous chemical discovery applications where experimental time and materials are valuable resources.

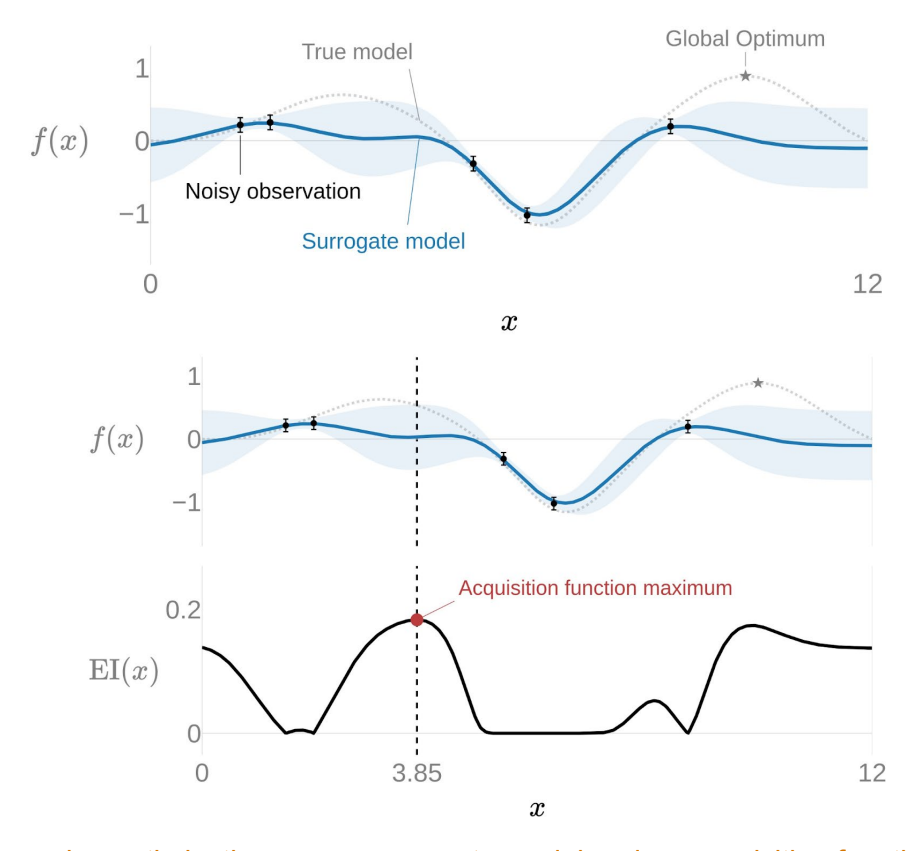


Figure 8. Bayesian optimization uses a surrogate model and an acquisition function to guide the search for optimal experiment conditions. Figure from ax.dev.

The optimization process operates through two key components: a surrogate model that learns from previous experiments and an acquisition function that determines the next experimental

conditions. Popular acquisition functions include Expected Improvement (EI), Upper Confidence Bound (UCB), and Probability of Improvement (PI), each offering different strategies for trading off exploration versus exploitation. As new experimental data becomes available, the surrogate model is updated using Bayesian inference, refining predictions and uncertainty estimates across the entire parameter space. Using an acquisition function like EI to sample new points initially promotes quick exploration because the expected values, informed by the uncertainty estimates, are higher in unexplored regions. Once the parameter space is adequately explored, EI naturally narrows focuses on regions where there is a high likelihood of a good objective value (i.e., exploitation). In our implementation, we used GP to model system outcomes and EI to optimize and suggest next experiments. These options (model type and acquisition function) can be varied in the configuration file. For details about GP and the acquisition functions, see Reference 5.

## 4.0 Large Language Models (LLMs) for Experiment Interpretation

We integrated large language models (LLMs) into ACE to translate raw sensor streams (such as IR spectra) to provide operationally meaningful narratives that guide the next experiment and make the Bayesian Optimizer's actions auditable and explainable. The key idea from our work is developing a two-phased approach, in which first we extract information about a reaction intermediate from spectral features, and then, we infer the present reaction state (e.g. under-excitation vs over-oxidation). This collective information and knowledge of intermediates coupled with the reaction state is next combined with the autonomy objective such as maximizing reaction yield to predict the next optimal experimental configuration.

### 4.1 Spectral Data Interpretation

Spectral feature extraction involves the following steps:

- 1) Identification of species from spectral features: The implementation of this step depends on our goals of focusing on a set of known intermediates versus open-ended extraction of possible candidates. We provide the experimental context as input to guide the LLM's reasoning about the presence of the species through reflectance, surface-enhanced adsorption etc. We also provide instructions to reason about data quality by attending to features such as baseline drift, signal-to-noise ratio, and interference fringes.
- 2) Next, we instruct the LLM to detect peaks with position, width, intensity and shape. Each detection needs to be associated with specific wavenumbers and mapped to specific phases (such as dissolved or gas-phase, modulation-excitation). Constraining the extraction step to produce incrementally richer features imposes strong reasoning requirements and leads to better qualitative results.
- 3) Collective disambiguation: Once obtaining a set of initial hypotheses (inside the LLM) regarding a set of intermediates, we reason at the functional group level in terms of their appearance in an experimentally observed context. We check for assignments based on prior expectations from literature and produce explanations in terms of mechanistic steps.

Fig. 9 provides an example of Al-based interpretation of IR spectroscopy data and its validation by a catalysis expert.

Spectral	AI Interpretation	Expert Evaluation	Assessment				
Feature							
Peak Assignments							
$1680  ext{ cm}^{-1}$ (dominant minimum)	C=O stretch with $\sim 35$ cm <sup>-1</sup> red-shift from free cyclohexanone. Indicates carbonyl	<b>Incorrect.</b> Broad feature from $H_2O/HO^-$ bending vibrations, not C=O stretch. Key distinc-	×				
	engaged in H-bonding to Brønsted acid or coordination to Lewis acid.	tion: C=O would be sharp; observed feature is very broad.					
1596 cm <sup>-1</sup> (secondary maximum)	Ring skeletal modes and/or residual H-O-H bend tail. Not diagnostic for alkoxide/enolate without 1200-900 cm <sup>-1</sup> region.	Partially correct. Also water bending mode, sensitive to pH- dependent H-bonding network. Baseline shift between product and reference spectra.	~				
Chemical Reasoning							
Structural Exclusions	Rules out: (i) Free cyclohexanone (would appear ~1715 cm <sup>-1</sup> ), (ii) Pure cyclohexanol on inert surface without carbonyl formation	<b>Correct.</b> Both exclusions are accurate based on spectroscopic evidence.	<b>√</b>				
Recommended Analysis	Additional spectral windows: 3200-3600 cm <sup>-1</sup> (O-H stretch), 1200-900 cm <sup>-1</sup> (C-O stretch) for alkoxide vs ketone distinction	Correct. Additional windows would provide decisive evidence. Note: 1200-900 cm <sup>-1</sup> region often complex.	<b>√</b>				

Figure 9. Expert evaluation of Al-extracted spectral features for cyclohexanol system

### 4.2 Suggesting Experimental Steps

We can model the experimental step prediction by constructing a state-space transition model of the reaction. Essentially, we formulate the autonomous steering problem into three substeps: 1) mapping the currently observed temporal experimental data into a high-level phase description and 2) then decide what is the optimal next phase for the reaction to pursue in accordance with the autonomy objective, and 3) search over the space of plausible actions to determine how to transition the chemical system from the current phase to the desired next phase.

We describe an example set of phase classifications below. This should be automatically generated by any state-of-the-art LLM in a reaction-specific fashion.

- Selective activation of the reactant: This is evidenced by observations of monotone growth
  and stabilization of the reaction rate. Our goal is to detect when the catalyst's interaction
  with reaction intermediates is neither too strong or weak to achieve highest activity (Sabatier
  principle). Observation of weak responses to small 10-20 mV steps would indicate underexcitation or barrier to entering the sweet spot.
- Over-oxidation: We reason about over-oxidation through seeking shift in characteristic band positions that correlates with the formation of oxidized metal species, and electron-deficient oxygen sites. This can be further improved through observation/constraining via change in peak intensity and shape, which informs us about the local bonding environment of oxygen atoms.

- Detecting Oxygen-evolution competition: As in above the key reasoning principles are
  identification and tracking the presence and concentration of different species and the
  change in their relative intensity. An initial observation of competition can be further verified
  through forcing the LLM to produce a mechanistic explanation such as change in vibrations
  of water or hydroxyl groups.
- Detection of de-activation/deposit accumulation: At this point, we can follow the general principle of making the LLM generate a) the phase definitions from a reaction, b) a list of candidate intermediates that indicate the formation of the phase (e.g. accumulation of carbonaceous deposits from C-H/C=O bands) and c) a list of mechanistic steps that we can reason about through observing the interaction (or lack of) of the candidates (such as disappearance of characteristic bands associated with active sites).

Given the inferred regime, suggestion of an experimental step is accomplished by prompting the LLM to select from a restricted action set. Again, these action spaces can be generated automatically by the LLM with domain-based verifications.

- Voltage step only: to move from under-excitation to steer towards "sweet spot". Confirm success of action through monotonic growth of product.
- Temperature step only: when mass transfer limits or deactivation suspected and rate/selectivity trends do not respond monotonically to voltage.
- No change: when we observe stable product yields and no evidence of deactivation.

## 5.0 User Experience (UX) Design

ACE's user interface development involved collaboration with a UX designer to create an intuitive front-end system that would lower the barrier to autonomous experimentation for researchers. The design focused on two primary components: an experiment specification interface and a real-time monitoring dashboard. The experiment specification module featured a form-based interface that guided users through parameter definition, objective selection, and constraint specification, with the intended capability to automatically generate the underlying YAML configuration files and associated Python metrics scripts. This approach aimed to eliminate the need for researchers to manually write configuration code while maintaining the flexibility of the underlying modular architecture.

The monitoring dashboard was designed to provide comprehensive oversight of autonomous experiments, displaying real-time optimization progress, current parameter values, and the operational status of all connected instruments including the potentiostat, temperature controller, and FTIR spectrometer. The dashboard incorporated visualization elements for tracking convergence metrics, experimental history, and system alerts to enable researchers to monitor long-running autonomous campaigns effectively. Throughout the design process, we conducted usability testing sessions with domain experts in electrochemistry and automation to validate interface concepts and refine user workflows based on their feedback. While significant progress was made in implementing core interface elements, development was ultimately redirected to prioritize the underlying automation infrastructure and algorithm validation across the chemistry campaigns. The partially implemented interface components provided valuable user experience insights that informed subsequent design decisions and established a foundation for future development efforts.

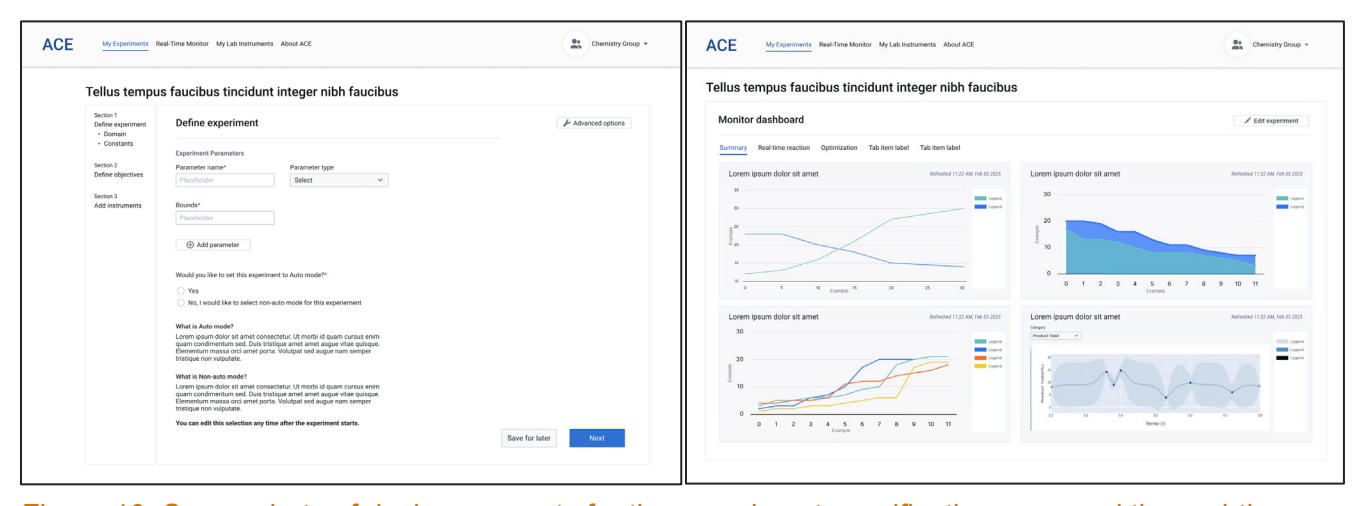


Figure 10. Screenshots of design concepts for the experiment specification page and the real-time dashboard.

### 6.0 Model Chemistries

Several different chemical reactions were selected for testing and demonstration of ACE (Figure 11.). Each of these reactions affords a product with a carbon-oxygen double bond that exhibits an intense stretching mode ( $v_{C=O}$ ) in the IR spectrum, which is ideal for detection during autonomous experimentation runs. Moreover, as discussed in the following sections, each reaction also presents a selectivity challenge that can benefit from the use of autonomous experimentation to identify the optimal conditions for the electrochemical reaction.

## 

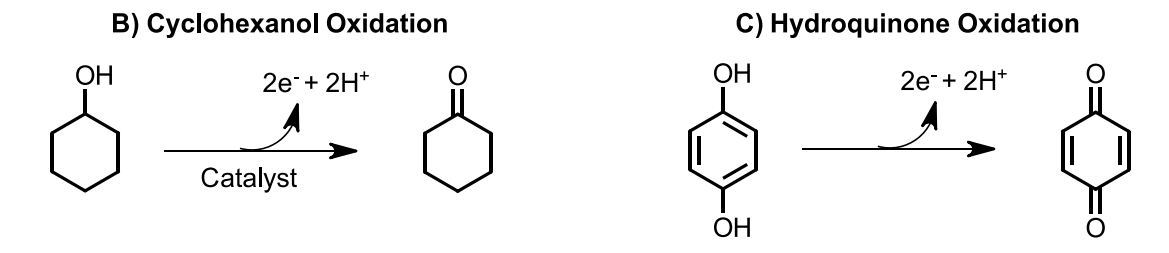


Figure 11. Depiction of the anode reactions selected for testing the autonomous electrochemistry platform. In each case, the corresponding cathode reaction is hydrogen evolution.

Significant challenges in product quantification were encountered for each of these reactions due to the detection limit of the FTIR probe. The aqueous electrolyte exhibited a noisy baseline, a pH-dependent bending mode in the spectral region of interest (1600-1700 cm<sup>-1</sup>), and significant variation in the overall shape of the baseline from one experiment to the next. To improve the data quality, we employed spectral averaging, smoothing functions, (Savitzky-Golay, moving average), and baseline correction routines (polynomial fits, AsLS). With these protocols, we found that product concentrations >10 mM could be reliably detected in calibration experiments, which is a much higher detection limit than expected for typically intense C=O stretching modes.

#### **6.1 Formate Oxidation**

The first reaction, catalytic oxidation of formate to bicarbonate, has been suggested as a reversible cycle for chemical storage and retrieval of dihydrogen. Oxidation of formate anion produces a mixture of bicarbonate and carbonate products as an acid/base pair that are in rapid equilibrium with each other. Therefore the ratio of products is determined by the solution pH, which in turn is impacted by the overall reaction conversion. Bicarbonate/carbonate can also decompose into carbon dioxide, which is not desirable for hydrogen storage applications due to the added complexity of capturing and storing a gaseous product. This leads to a selectivity challenge, in which catalytic systems are needed that can selectively oxidize formate to bicarbonate instead of carbon dioxide.

Model Chemistries 15

One challenge of the formate oxidation reaction is that both the reactant and products exhibit multiple symmetric and asymmetric stretching bands in the IR spectra (Figure 12). This presented a challenge for quantification of overlapping signals. To address this challenge, we employed the initial potassium formate spectrum as a baseline reference, featuring a characteristic peak at 1576 cm<sup>-1</sup>. This approach enabled real-time monitoring of reactant consumption through the progressive decrease of the 1576 cm<sup>-1</sup> peak intensity, while simultaneously tracking the formation of bicarbonate (1652 cm<sup>-1</sup>) and carbonate (1404 cm<sup>-1</sup>) products at different applied potentials and temperatures.

Figure 12. Calibration curves obtained from FTIR response for known concentrations of potassium formate (left) and potassium bi-carbonate (right) aqueous solutions.

## **6.2 Cyclohexanol Oxidation**

The second reaction, catalytic oxidation of cyclohexanol to cyclohexanone, was selected as a model reaction with simpler product analysis as the mid-IR spectral region contains a single symmetric  $v_{C=O}$  band for the product and no bands for the reactant. Some catalysts can further oxidize cyclohexanone to adipate through C-C bond cleavage and ring opening.<sup>8-9</sup> The reaction mechanisms dictating selectivity for one product over the other are not well understood. As a result, autonomous experimentation is a promising avenue to rapidly identify how the experimental conditions can steer a given catalyst to favor one product over the other.

Model Chemistries 16

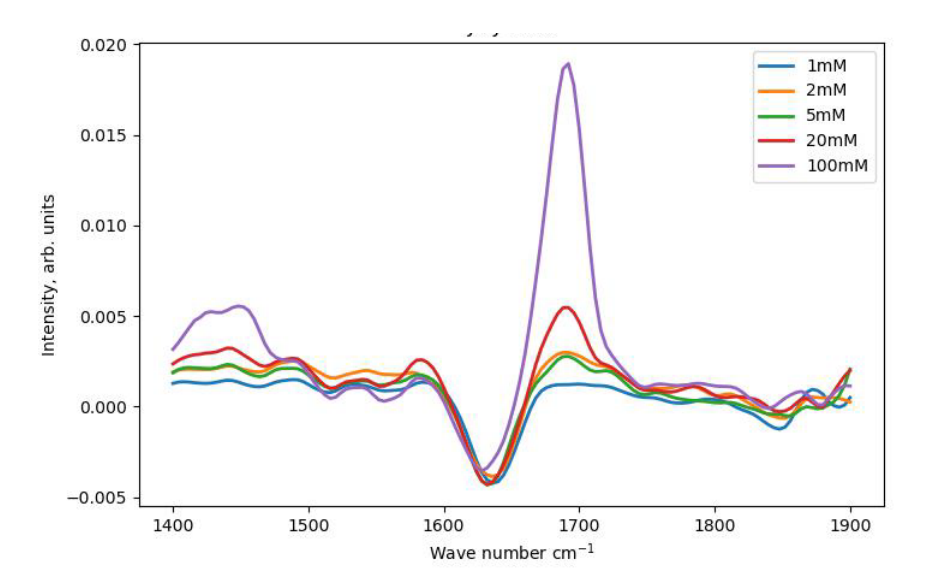


Figure 13: Calibration curves obtained from FTIR response for known concentrations of cyclohexanone aqueous solutions.

## 6.3 Hydroquinone Oxidation

The final reaction, oxidation of hydroquinone to benzoquinone, has been studied for applications in organic redox flow batteries, 10-11 mediated fuel cells, 12 and pH-swing separations. 13 This reaction occurs facilely at an electrode in the absence of a catalyst, 14 such that the reaction may display much higher rates and conversions than either catalytic oxidation of formate or cyclohexanol. However, hydroquinone can also be electrochemically polymerized under some conditions, 15-16 creating a selectivity challenge that that can potentially be overcome using autonomous reaction optimization.

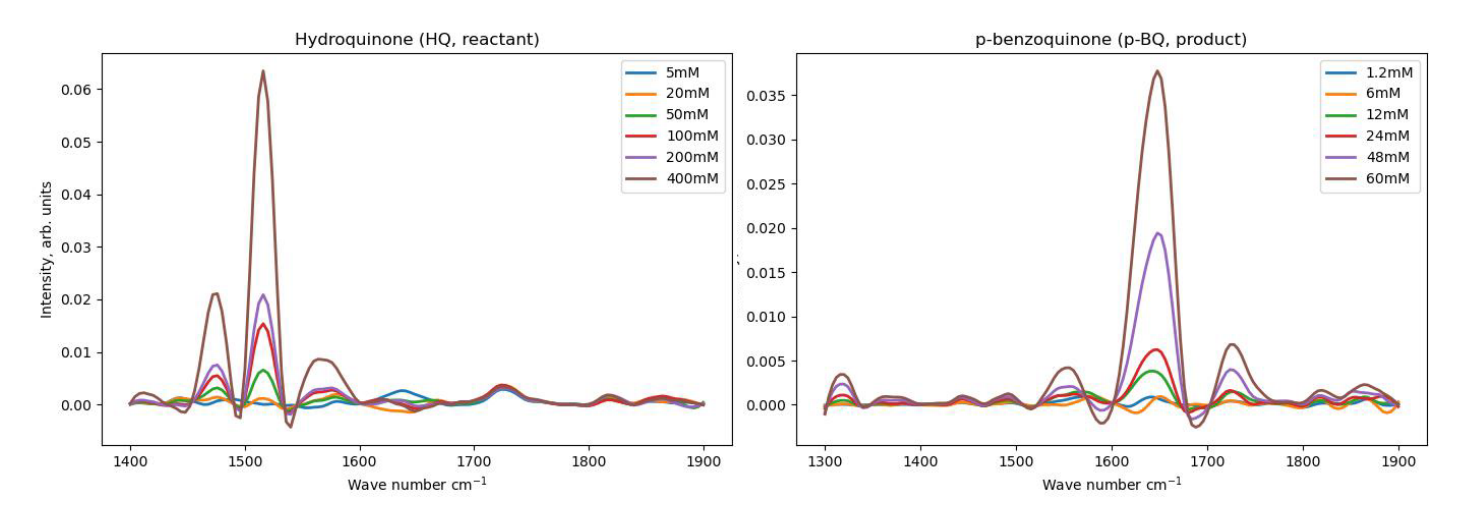


Figure 14: Calibration curves obtained from FTIR response for known concentrations of hydroquinone (left) and benzoquinone (right) aqueous solutions.

Model Chemistries 17

## 7.0 Experimentation Procedure

ACE was incrementally developed from semi-autonomous to fully autonomous experimentation, beginning with a human-in-the-loop configuration that provided a controlled transition toward complete automation.

### 7.1 Human-in-the-loop Experimentation (FY 24)

## Figure 15: Human-in-the-loop, semi-autonomous workflow with two distinct points of human intervention.

In this initial setup, ACE functioned as an intelligent decision-making system while relying on minimal human intervention for specific manual tasks that had not yet been automated. Initial experiments were conducted by varying applied voltage at ambient room temperature to reduce system complexity, with temperature control subsequently incorporated as an additional design variable in later experiments. The semi-autonomous workflow is as follows:

- Initial Condition Generation: ACE's optimization algorithm suggests initial experimental
  conditions (voltage setpoints and later temperature targets) based on the defined parameter
  space and objectives specified in the YAML configuration file. Recommended experimental
  conditions are communicated to the experimentalist.
- Manual Instrument Configuration (first point of human intervention): Researcher
  manually configures the potentiostat with ACE-specified voltage settings and starts data
  collection on ReactIR FTIR spectrometer to continuously collect time-series measurements at
  regular intervals, automatically saving spectral data to pre-specified directory.
- **Reaction Execution:** Electrochemical reaction proceeds autonomously for predetermined 24-hour duration.

- Data Transfer (second point of human intervention): Upon experiment completion, the
  researcher moves time-series spectra data to network drive. This intervention was necessary
  because the FTIR's proprietary software does not allow direct saving of spectra files to a
  network drive.
- Autonomous Decision-Making: ACE's data processing pipeline activates automatically
  within seconds to: (i) Import raw spectral files, (ii) Apply preprocessing algorithms, (iii)
  Compute performance metrics, (iv) Execute Bayesian optimization algorithm to determine the
  next set of experimental conditions.
- **Researcher Notification:** Researcher receives alert with newly proposed parameter values for subsequent experiment cycle.

This human-in-the-loop approach required only two discrete points of manual intervention: initial instrument configuration with ACE-specified voltage settings and transfer of FTIR data files to designated analysis directories. All aspects of experimental design, data interpretation, performance evaluation, and optimization-based decision making were handled autonomously by ACE, demonstrating the system's capability to manage the complete experimental reasoning loop while maintaining compatibility with existing laboratory infrastructure and workflows.

### 7.2 Autonomous Experimentation

The fully autonomous configuration eliminated both points of human intervention identified in the human-in-the-loop setup, enabling ACE to directly control all experimental instruments and execute complete optimization cycles without manual oversight. To enable this advanced operational mode, a flow reactor replaced the batch reactor and ACE maintained direct communication with both the potentiostat and temperature controller, automatically implementing voltage and temperature setpoints as determined by the Bayesian optimization algorithm. All variables, parameters, and objectives remain specified in the same YAML configuration file

Figure 16: Fully autonomous workflow with direct instrument control.

format, with identical data processing and metrics computation scripts used in the human-in-the-loop configuration. The fully autonomous experimentation workflow is as follows:

- **Experiment Initialization:** Electrolyte flow is initiated through the flow cell, ReactIR FTIR spectrometer begins data collection, and the autonomous experiment sequence commences.
- **Electrochemical Characterization:** ACE executes cyclic voltammetry technique via the potentiostat to perform initial electrochemical characterization, automatically determining suitable voltage ranges based on reasonable current response values. Temperature control range is fixed between 25°C (room temperature) and 65°C as specified in configuration file.
- **Initial Condition Generation:** Bayesian optimization algorithm autonomously selects starting experimental conditions (voltage and temperature setpoints)
- **Direct Instrument Control:** ACE runs the following sequence of techniques on the potentiostat to set the new voltage: (i) Potentiostatic Electrochemical Impedance Spectroscopy, (ii) Ohmic drop compensation, (iii) Chronoamperometry. ACE also sets the temperature setpoint.
- **Equilibration Phase:** A 10-minute stabilization period allows both electrochemical and thermal systems to reach steady-state conditions at target setpoints.
- **Data Collection Phase:** A 2-minute FTIR data acquisition is performed while maintaining constant experimental conditions (voltage and temperature)
- **Data Processing and Analysis:** (i) FTIR spectral data is automatically averaged across the 2-minute collection window, (ii) Product quantification is performed using pre-established calibration relationships, (iii) Key performance metrics are computed from processed spectral data.
- Optimization Decision: Bayesian optimization algorithm processes computed metrics to determine next optimal experimental conditions. Process repeats autonomously with new voltage and temperature setpoints until convergence criteria are met or maximum iterations reached.

This fully autonomous workflow requires zero human intervention after initiating the experiment sequence, demonstrating ACE's capability for unattended optimization cycles spanning multiple hours (or even days) while maintaining precise experimental control and data quality standards.

## 8.0 Key Optimization Metrics

The ACE platform evaluated electrocatalytic performance using four critical metrics that comprehensively assess reaction efficiency, selectivity, and kinetics. These metrics provided quantitative objectives for Bayesian optimization while enabling meaningful comparison across different experimental conditions and chemistry campaigns.

### 8.1 Product Yield

Product yield quantifies the conversion efficiency of reactant to desired product, expressed as:

$$Y = \frac{n_{\text{product}}}{n_{\text{reactant.initial}}} \times 100\%$$

where  $n_{\rm product}$  represents moles of target product formed and  $n_{\rm reactant,\;initial}$  is the initial moles of reactant.

### **Derivation from Experimental Data:**

- FTIR Analysis: Product concentrations were determined using relationships established through offline calibration curves. Peak areas corresponding to characteristic vibrational modes were integrated and converted to concentration using pre-established calibration factors.
- **Batch Setup:** Initial reactant concentration was known from solution preparation. Final product concentration was measured after 24-hour reaction completion.
- **Flow Setup:** Steady-state product concentration was measured during the 2-minute data collection window, with reactant concentration determined from inlet flow composition.

## 8.2 Faradaic Efficiency

Faradaic efficiency measures the fraction of total charge that contributes to the desired electrochemical reaction, calculated as:

$$FE = \frac{n \times z \times F}{Q_{\text{total}}} \times 100\%$$

where n is moles of product, z is electrons transferred per molecule of product (z=2, for a 2-electron reaction), F is Faraday's constant (96,485 C/mol), and  $Q_{\text{total}}$  is total charge passed.

### **Derivation from Experimental Data:**

- **Electrochemical Readouts:** Total charge was calculated by integrating current over time:  $Q = \int I(t) dt$
- **FTIR Quantification:** Product moles determined from spectroscopic analysis and calibration relationships
- Batch Setup: Charge integration performed over entire 24-hour reaction period

• Flow Setup: Steady-state current measured during the 2-minute data collection window, with charge calculated for sampling interval of 1s. The total product was computed from FTIR quantification and volumetric flow rate (L/s).

### 8.3 Selectivity

Selectivity evaluates the preference for desired product formation relative to competing side reactions:

$$S = rac{n_{ ext{target product}}}{\sum n_{ ext{all products}}} imes 100\%$$

### **Derivation from Experimental Data:**

- FTIR Multi-component Analysis: Simultaneous quantification of all detectable products using their characteristic absorption bands
- Calibration Requirements: Individual calibration curves established for each potential product species

### 8.4 Reaction Rate

Reaction rate quantifies the speed of product formation, normalized to either reactor volume or electrode surface area:

$$r = \frac{dn_{\text{product}}}{dt \times V} \text{ or } \frac{dn_{\text{product}}}{dt \times A}$$

where *V* is reactor volume and *A* is electrode surface area.

### **Derivation from Experimental Data:**

- Batch Setup: Rate calculated from concentration change over 24-hour period:  $r = \frac{[P]_{\text{final}} [P]_{\text{initial}}}{t \times V}$
- Flow Setup: Steady-state rate determined from residence time analysis:  $r=\frac{[P]_{\text{out}}\times\dot{V}}{V_{\text{reactor}}}$  where  $\dot{V}$  is volumetric flow rate
- **FTIR Integration:** Product concentration profiles enabled rate determination through numerical differentiation of concentration-time relationships

While all four metrics were computed and monitored for every reaction, the Bayesian optimization algorithm focused exclusively on product yield and current efficiency (Faradaic efficiency) as the primary objectives for autonomous decision-making. This strategic selection simplified the multi-objective optimization problem while targeting the most critical performance indicators for electrocatalytic processes, consistent with established practices in autonomous electrochemical experimentation.

## 9.0 Key Results

## 9.1 FY24 (Level 3) Human-in-the-loop experimentation

Prior to initiating the effort to automate the flow reactor, a human-in-the-loop experiment was conducted to verify that the Bayesian optimization implementation was working as expected. For this experiment, a Pd/carbon anode was used to catalyze the oxidation of formate to bicarbonate using the stirred batch reactor. As described above, the FTIR spectra of this reaction exhibit strongly overlapping bands from 1200-1800 cm<sup>-1</sup>, which could be addressed using the initial formate solution as the baseline for the experimental data. Representative time-series data for the reaction progression for optimal conditions are shown in Figure 17.

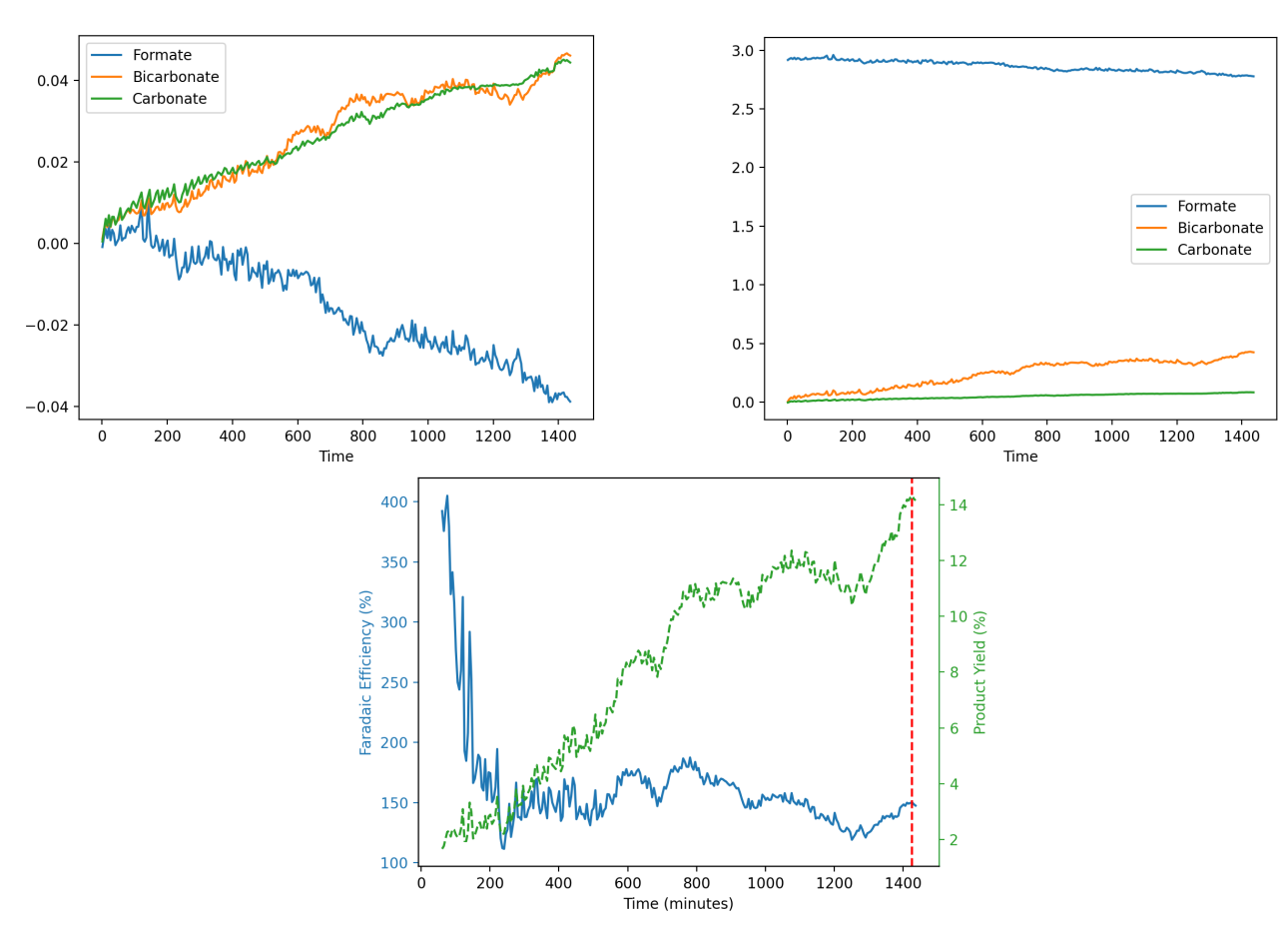


Figure 17: Product quantification and key metrics of catalytic formate oxidation, showing the time dependence of FTIR signal intensity (top left), calculated concentrations (top right), and the catalytic metrics of Product Yield and Faradaic Efficiency (bottom).

Key Results 23

The optimization campaign was carried out by varying a single parameter (electrode potential) and monitoring the impact on the product yield and Faradaic efficiency after 24 hours of reaction. The Bayesian Optimizer successfully narrowed into an optimal potential, ~0.36 V, after sampling only eight different electrode potentials. This can be seen visually in Figure 18, where the optimum potential is characterized by a low uncertainty of the two optimization objectives.

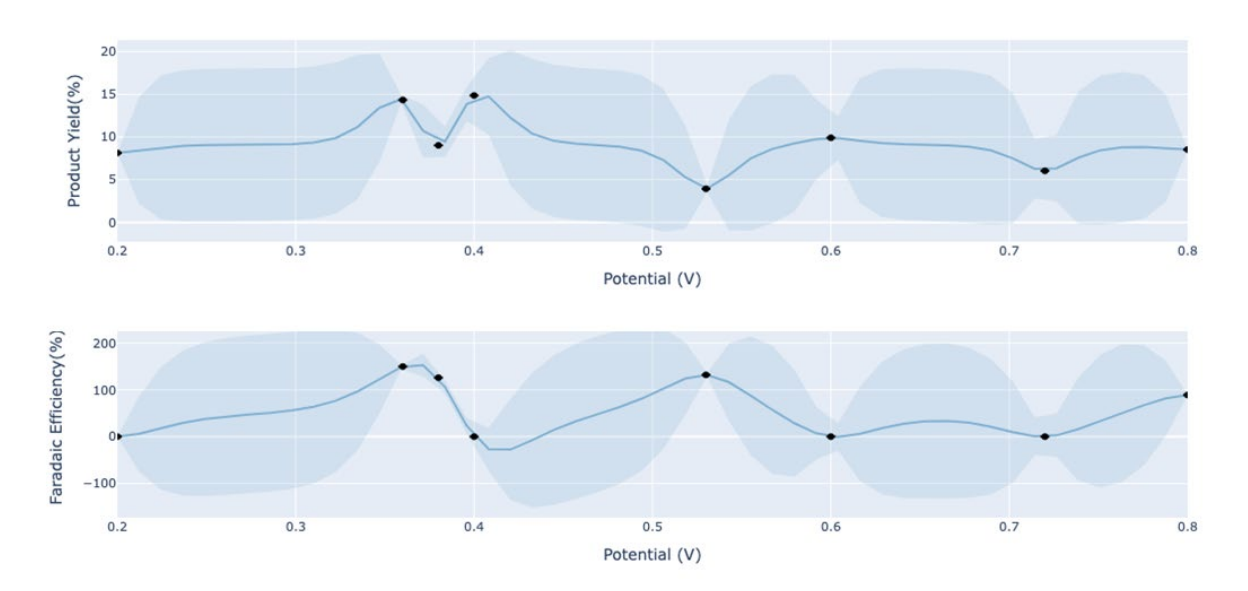


Figure 18: Evolution of Gaussian process surrogate model used by the multi-objective Bayesian optimization algorithm. After 8 runs, the optimal potential was found around 0.36V.

## 9.2 FY25 (Level 4) Autonomous Experimentation

Fully autonomous experiments were conducted for catalytic oxidation of formate and cyclohexanol. In these experiments, the flow reactor was configured for single pass measurements to simplify the automation requirements and enable real-time measurements. However, the catalysts we tested did not exhibit high enough activity to generate sufficient product in a single pass for detection by the FTIR. To address these sensitivity limitations, we pivoted to the non-catalytic electrochemical oxidation of hydroquinone to p-benzoquinone, which provided higher conversion rates suitable for online detection. Initial attempts to monitor the characteristic carbonyl stretch at 1652 cm<sup>-1</sup> were confounded by overlap with the water bending mode. Consequently, we recalibrated our analytical approach using the less intense but spectrally isolated peak at 1318 cm<sup>-1</sup>, establishing new calibration curves for product quantification.

Process optimization revealed critical operating constraints and system limitations. Certain voltage-temperature combinations (above unknown threshold values) induced undesired polymerization reactions, manifesting as precipitate formation that occluded flow channels and polymer deposition on the titanium electrode surface. This electrode fouling significantly impeded current generation, resulting in diminished product yields and compromised electrochemical performance. Additionally, the reactor's thermal control system, equipped only with a heating

Key Results 24

element and lacking active cooling capability, created significant temperature equilibration delays. Once elevated temperatures were reached, the system required extended periods to cool to lower setpoints, severely constraining the autonomous optimization algorithm's ability to efficiently explore the temperature parameter space. Future system iterations will require integrated cooling mechanisms to enable rapid bidirectional temperature control.

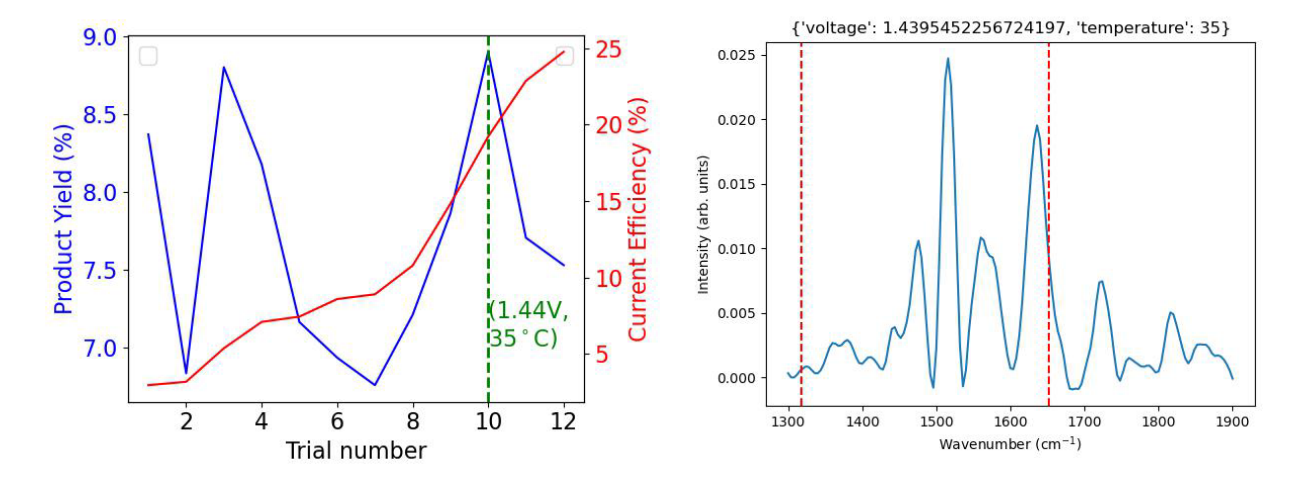


Figure 19: Evolution of key metrics - product yield and current efficiency for the hydroquinone oxidation reaction (left) corresponding IR spectra (right). The water peak near 1652 cm<sup>-1</sup> overlaps with the product peak. For quantification, we used the peak at 1318 cm<sup>-1</sup> to enable optimization decisions. The optimal conditions over 12 trials were 1.44V and 35°C.

These trials successfully demonstrated ACE's autonomous decision-making capabilities, including real-time parameter adjustment and adaptive experimental design without human intervention. However, the results highlight the need for improved chemistry execution protocols and enhanced thermal management systems to achieve reliable product quantification in autonomous workflows. Future iterations will focus on expanding the viable chemistry space, implementing predictive models to avoid deleterious operating conditions, and incorporating active cooling systems for comprehensive temperature control.

Key Results 25

### 10.0 Conclusion

In summary, this project successfully achieved autonomous experimentation of flow electrosynthesis for several different model chemistries. Multiple technical milestones were achieved during this project, including the development of a robust automation platform, an extensible modular workflow, and demonstration of both human-in-the-loop (L3) autonomy and high (L4) autonomy. Our efforts in this area have been presented in two community workshops – "AI/ML for Isotopes" at Los Alamos National Laboratory, and "Scientific Discovery in the AI Age" at Argonne National Laboratory and multiple internal research symposia. Finally, our success in this LDRD project has enabled us to secure follow-on funding from DOE ASCR (FWP 86405) and has elicited strong internal collaboration interest. These outcomes emphasize the potential for ACE to enable greater experimental autonomy for a variety of energy-scale chemical challenges.

Conclusion 26

### 11.0 References

- 1. Bhatwadekar, S.; Boruah, B.; Riedel, N. W.; Royer, N. D.; Pedersen, T. H.; Lopez-Ruiz, J. A. Electrocatalytic oxidation of hydrothermal liquefaction-derived aqueous phase for on-site wastewater treatment and H<sub>2</sub> production. *Cell Reports Physical Science* **2025**, *6*. DOI:https://dx.doi.org/10.1016/j.xcrp.2025.102555.
- 2. Andrews, E.; Lopez-Ruiz, J. A.; Egbert, J. D.; Koh, K.; Sanyal, U.; Song, M.; Li, D.; Karkamkar, A. J.; Derewinski, M. A.; Holladay, J.; Gutiérrez, O. Y.; Holladay, J. D. Performance of Base and Noble Metals for Electrocatalytic Hydrogenation of Bio-Oil-Derived Oxygenated Compounds. *ACS Sustainable Chem. Eng.* **2020**, *8*, 4407-4418. DOI:https://dx.doi.org/10.1021/acssuschemeng.9b07041.
- 3. Lopez-Ruiz, J. A.; Andrews, E. M.; Akhade, S. A.; Lee, M.-S.; Koh, K.; Sanyal, U.; Yuk, S. F.; Karkamkar, A. J.; Derewinski, M. A.; Holladay, J.; Glezakou, V.-A.; Rousseau, R.; Gutiérrez, O. Y.; Holladay, J. D. Understanding the role of metal and molecular structure on the electrocatalytic hydrogenation of oxygenated organic compounds. *ACS Catal.* **2019**. DOI:https://dx.doi.org/10.1021/acscatal.9b02921.
- 4. Lopez-Ruiz, J. A.; Sanyal, U.; Egbert, J.; Gutiérrez, O. Y.; Holladay, J. Kinetic Investigation of the Sustainable Electrocatalytic Hydrogenation of Benzaldehyde on Pd/C: Effect of Electrolyte Composition and Half-Cell Potentials. *ACS Sustainable Chem. Eng.* **2018**, 6, 16073-16085. DOI:https://dx.doi.org/10.1021/acssuschemeng.8b02637.
- 5. Shahriari, B.; Swersky, K.; Wang, Z.; Adams, R. P.; Freitas, N. d. Taking the Human Out of the Loop: A Review of Bayesian Optimization. *Proceedings of the IEEE* **2016**, *104*, 148-175. DOI:https://dx.doi.org/10.1109/JPROC.2015.2494218.
- 6. Grubel, K.; Jeong, H.; Yoon, C. W.; Autrey, T. Challenges and opportunities for using formate to store, transport, and use hydrogen. *J. Energy Chem.* **2020**, *41*, 216-224. DOI:https://dx.doi.org/https://doi.org/10.1016/j.jechem.2019.05.016.
- 7. Grubel, K.; Su, J.; Kothandaraman, J.; Brooks, K.; Somorjai, G. A.; Autrey, T. Research Requirements to Move the Bar forward Using Aqueous Formate Salts as H<sub>2</sub> Carriers for Energy Storage Applications. *Journal of Energy and Power Technology* **2020**, *02*, 016. DOI:https://dx.doi.org/10.21926/jept.2004016.
- 8. Jia, Y.; Chen, Z.; Gao, B.; Liu, Z.; Yan, T.; Gui, Z.; Liao, X.; Zhang, W.; Gao, Q.; Zhang, Y.; Xu, X.; Tang, Y. Directional Electrosynthesis of Adipic Acid and Cyclohexanone by Controlling the Active Sites on NiOOH. *J. Am. Chem. Soc.* **2024**, *146*, 1282-1293. DOI:https://dx.doi.org/10.1021/jacs.3c05898.
- 9. Li, Z.; Li, X.; Zhou, H.; Xu, Y.; Xu, S.-M.; Ren, Y.; Yan, Y.; Yang, J.; Ji, K.; Li, L.; Xu, M.; Shao, M.; Kong, X.; Sun, X.; Duan, H. Electrocatalytic synthesis of adipic acid coupled with H<sub>2</sub> production enhanced by a ligand modification strategy. *Nat. Commun.* **2022**, *13*, 5009. DOI:https://dx.doi.org/10.1038/s41467-022-32769-0.
- 10. Gerken, J. B.; Anson, C. W.; Preger, Y.; Symons, P. G.; Genders, J. D.; Qiu, Y.; Li, W.; Root, T. W.; Stahl, S. S. Comparison of Quinone-Based Catholytes for Aqueous Redox Flow Batteries and Demonstration of Long-Term Stability with Tetrasubstituted Quinones. *Adv. Energy Mater.* **2020**, *10*, 2000340. DOI: <a href="https://dx.doi.org/10.1002/aenm.202000340">https://dx.doi.org/10.1002/aenm.202000340</a>.
- 11. Wang, C.; Yang, Z.; Wang, Y.; Zhao, P.; Yan, W.; Zhu, G.; Ma, L.; Yu, B.; Wang, L.; Li, G.; Liu, J.; Jin, Z. High-Performance Alkaline Organic Redox Flow Batteries Based on 2-Hydroxy-3-carboxy-1,4-naphthoquinone. *ACS Energy Lett.* **2018**, 3, 2404-2409. DOI:https://dx.doi.org/10.1021/acsenergylett.8b01296.
- 12. Anson, C. W.; Stahl, S. S. Mediated Fuel Cells: Soluble Redox Mediators and Their Applications to Electrochemical Reduction of O<sub>2</sub> and Oxidation of H<sub>2</sub>, Alcohols, Biomass, and Complex Fuels. *Chem. Rev.* **2020**, *120*, 3749-3786. DOI:https://dx.doi.org/10.1021/acs.chemrev.9b00717.

References 27

- 13. Huang, C.; Liu, C.; Wu, K.; Yue, H.; Tang, S.; Lu, H.; Liang, B. CO<sub>2</sub> Capture from Flue Gas Using an Electrochemically Reversible Hydroquinone/Quinone Solution. *Energy Fuels* **2019**, *33*, 3380-3389. DOI:https://dx.doi.org/10.1021/acs.energyfuels.8b04419.
- 14. Huynh, M. T.; Anson, C. W.; Cavell, A. C.; Stahl, S. S.; Hammes-Schiffer, S. Quinone 1 e<sup>-</sup> and 2 e<sup>-</sup>/2 H<sup>+</sup> Reduction Potentials: Identification and Analysis of Deviations from Systematic Scaling Relationships. *J. Am. Chem. Soc.* **2016**, *138*, 15903-15910. DOI:https://dx.doi.org/10.1021/jacs.6b05797.
- 15. Foos, J. S.; Erker, S. M.; Rembetsy, L. M. Synthesis and Characterization of Semiconductive Poly-1,4-Dimethoxybenzene and Its Derived Polyquinone. *J. Electrochem. Soc.* **1986**, *133*, 836. DOI:https://dx.doi.org/10.1149/1.2108689.
- 16. Pham, M.-C.; Hachemi, A.; Dubois, J.-E. An apparently totally electroactive polymer film obtained by electropolymerizing 5-hydroxy-1,4-naphthoquinone onto graphite. *J. Electroanal. Chem.* **1984**, *161*, 199-204. DOI: <a href="https://dx.doi.org/https://doi.org/10.1016/S0022-0728(84)80262-4">https://dx.doi.org/https://doi.org/10.1016/S0022-0728(84)80262-4</a>.

References 28

# Pacific Northwest National Laboratory

902 Battelle Boulevard P.O. Box 999 Richland, WA 99354

1-888-375-PNNL (7665)

www.pnnl.gov